

A modified linear-mixing method for calculating atmospheric path radiances of aerosol mixtures

W. A. Abdou, J. V. Martonchik, R. A. Kahn, R. A. West, and D. J. Diner
Jet Propulsion Laboratory, California Institute of Technology

(June 24, 1996)

Abstract

The top-of-atmosphere (TOA) path radiance generated by an aerosol mixture can be synthesized by linearly adding the contributions of the individual aerosol components, weighted by their fractional optical depths. The method, known as linear mixing, is exact in the single-scattering limit. When multiple scattering is significant, the method reproduces the atmospheric path radiance of the mixture with < 3% errors for weakly absorbing aerosols up to optical thickness of 0.5. However, when strongly absorbing aerosols are included in the mixture, the method fails. This is due to neglecting the effect of multiple interactions between the aerosol components, especially when the values of the single scattering albedos of these components are so different that the parameter $\epsilon = \sum f_i |\omega_i - \omega_{mix}| / \omega_i$ is larger than -0.1, where ω_i and f_i are the single scattering albedo and the fractional abundance of the i^{th} component, and ω_{mix} is the effective single scattering albedo of the mixture. We describe an empirical, modified linear-mixing method which effectively accounts for the multiple interactions between aerosol components. The modified and standard methods are identical when $\epsilon = 0.0$, and give similar results when $\epsilon \leq 0.05$. For optical depths larger than -0.5, or when $\epsilon > 0.05$, only the modified method can reproduce the radiances within 5% error for common aerosol types up to optical thickness of 2.0. Because this method facilitates efficient and accurate atmospheric path radiance calculations for mixtures of a wide variety of aerosol types, it will be used as part of the aerosol retrieval methodology for the Earth Observing System (EOS) Multi-angle Imaging SpectroRadiometer (MISR), scheduled for launch into polar orbit in 1998.

Introduction

In a recent work by Wang and Gordon [1994] a method of linear mixing is described by which the aerosol contribution to the top-of-atmosphere (TOA) radiance, L , over ocean is synthesized from radiances generated from individual components of the aerosol, each with a unique size distribution or refractive index. The TOA radiance for an atmosphere above a black surface, i.e., the atmospheric path radiance, can be expressed as an equivalent reflectance p , defined as $p = \pi L / E_0$, where E_0 is the exo-atmospheric solar irradiance. The atmospheric path equivalent reflectance, p , is expressed in the linear mixing method as:

$$\rho(-\mu, \mu_0, \Delta\phi, \lambda, \tau_a) = \sum_{i=1}^n f_i \rho_i(-\mu, \mu_0, \Delta\phi, \lambda, \tau_a) \quad , \quad (1)$$

where, μ and μ_0 are the cosines of the viewing and sun angles, θ and θ_0 , respectively, with the negative sign in μ indicating upwelling radiation, $\Delta\phi = \phi - \phi_0$ is the view azimuthal angle with respect to the sun position, λ is the wavelength, τ_a is the total aerosol optical depth, n is the total number of components in the mixture, ρ_i is the atmospheric path equivalent reflectance of the i^{th} aerosol component, and f_i is its fractional contribution to the total aerosol optical thickness, τ_a , i.e.,

$$f_i = \frac{\tau_i}{\tau_a} \quad , \quad (2)$$

where,

$$\tau_a = \sum_{i=1}^n \tau_i \quad , \quad (3)$$

and τ_i is the optical thickness of the i^{th} component in the mixture. In Eq. (1), each ρ_i includes the contribution of Rayleigh scattering. Note that a key feature of the linear mixing approach is the evaluation of each ρ_i at the optical depth corresponding to the total column amount, τ_a .

The errors in calculating the atmospheric path radiance by Eq. (1) are estimated by comparing p to a "true" value. This value, ρ_t , is evaluated by radiative transfer calculations, using an effective single scattering albedo, ω_{mix} , and phase function, p_{mix} , for the mixture, expressed as:

$$\omega_{mix}(\lambda) = \sum_{i=1}^n f_i(\lambda) \omega_i(\lambda) \quad , \quad (4)$$

and

$$p_{mix}(\Omega, \lambda) = \sum_{i=1}^n \frac{f_i(\lambda) \omega_i(\lambda) p_i(\Omega, \lambda)}{\omega_{mix}(\lambda)} \quad , \quad (5)$$

where ω_i and p_i are the single scattering albedo and phase function, respectively, of the i^{th} aerosol component, and Ω is the scattering angle.

As explained by Wang and Gordon [1994], Eq. (1) is exact in the single-scattering limit, where light is scattered only once by one particle, and the contribution to the single-scattering radiance from each aerosol component, i , is exactly equal to ρ_i weighted by its fractional content in the mixture. Even when multiple scattering is significant, Wang and Gordon were able to reproduce p , using Eq. (1), with errors less than ~3%, for weakly-absorbing aerosols, and optical thickness ≤ 0.5 .

For strongly absorbing aerosols, they reported larger errors and, sometimes, the method failed. Our investigation shows that the method fails under such conditions because it does not account for the multiple interactions among the different aerosol types in the mixture.

In the case of multiple-scattering within aerosol mixtures, light is scattered by particles with potentially different scattering and absorbing characteristics. If the single scattering albedos of the different aerosol components are nearly equal, or more specifically, if

$$\epsilon(\lambda) = \sum_{i=1}^n \frac{f_i |\omega_i(\lambda) - \omega_{mix}(\lambda)|}{\omega_i(\lambda)}, \quad (6)$$

is small enough (e.g., < 0.05), then the radiances contributed by the individual components are not altered significantly due to the different scattering characteristics of the other components. In this case, which may also include strongly absorbing mixtures, Eq. (1) remains a good approximation. On the other hand, if $\epsilon \geq 0.1$, which is usually the case if one component is strongly absorbing relative to the others, the radiances contributed by the weakly absorbing components will be effectively attenuated due to the presence of the strongly absorbing components. Similarly, the contributions of the more absorbing components will be less attenuated due to the presence of the weakly absorbing ones. In such cases, the standard linear-mixing method fails.

In the following section we present a modified linear-mixing formula which empirically accounts for the mutual interactions between the various aerosol types present in a mixture and is capable of reproducing the atmospheric path radiance with errors $< 5\%$ for a variety of natural aerosol types, up to optical thickness of 2.0, for a wide range of viewing and illumination geometries.

Modified Linear-Mixing Method

Since standard linear-mixing is exact in the single-scattering limit, we separate the calculated atmospheric path equivalent reflectance into the single-scattered part, ρ_{ss} , and the multiple-scattered part, ρ_{ms} , i.e.,

$$\rho = \rho_{ss} + \rho_{ms}, \quad (7)$$

The standard method, expressed by Eq. (1), is used to calculate ρ_{ss} , i.e.,

$$\rho_{ss} = \sum_{i=1}^n f_i \rho_{i,ss}, \quad (8)$$

where, for convenience, the dependencies on $\mu, \mu_0, \Delta\phi, \lambda,$ and τ_a , are not explicitly shown here and in subsequent equations. The multiply scattered part, ρ_{ms} , is calculated by a modified linear-mixing method, using the following semi-empirical formula:

$$\rho_{ms} = \rho_{r,ms} + \sum_{i=1}^n \frac{\omega_{mix}}{\omega_i} e^{-\tau_a |\omega_i - \omega_{mix}|} f_i(\rho_{i,ms} - \rho_{r,ms}) \quad (9)$$

where $\rho_{r,ms}$ is the multiply scattered part of the atmospheric path equivalent reflectance due to Rayleigh-scattering. Its single-scattering part, $\rho_{r,ss}$ is included in $\rho_{i,ss}$ of Eq. (8). The function $\rho_{i,ms}$ is the multiply scattered part of p from the i^{th} aerosol component, including the multiple-scattered Rayleigh contribution. The Rayleigh contribution, ρ_r , is calculated in absence of the aerosol layer, at an optical depth, τ_r , which corresponds to the given wavelength and surface pressure. The exponential term in Eq.(9) approximates the attenuation caused by the presence of strongly absorbing components, whereas the ratio ω_{mix}/ω_i accounts for the reverse effect as explained in the previous section.

In the special case when all components in the mixture have the same single scattering albedo, and therefore, $\omega_i = \omega_{mix}$, we have $\epsilon = 0.0$, and Eqs. (7), (8), and (9) reduce to Eq. (1), and the standard and modified linear-mixing approaches are identical. The calculations and results, presented in next section, show that when $0.0 \leq \epsilon < 0.05$, both methods give similar results, with errors $< 5\%$, up to optical thickness of -2 . Whenever $\epsilon > 0.05$, only the modified method can achieve this accuracy.

The Calculations

The modified linear-mixing method was developed essentially to be used in retrieving the aerosol properties and optical depth from observations with the Multi-angle imaging Spectroradiometer (MISR) [Diner et al., 1991], scheduled to be flown on the Earth Observing System (EOS) AM platform in 1998. MISR is a multi-angle push-broom imaging system which acquires data with a 360-km swath at nine view directions in four spectral bands. MISR's retrieval method for aerosol properties [Diner et al., 1995] is based on comparing equivalent reflectances derived from the observed radiances to values simulated by a representative set of aerosol models which are likely to exist in the Earth's atmosphere. The simulated data are being generated by a doubling-adding radiative transfer code based on the method of Hansen and Travis [1974]. The calculations are made at predetermined sets of values for all the variables which affect MISR's observations, including mixes of 5 compositional types of naturally-occurring particles, some specified with coarse and accumulation mode size distributions. It would be difficult to store and access simulated MISR radiances for all possible mixes of these particle types. However, using the modified linear-mixing method, the size of the simulated data set is reduced dramatically by limiting its content to only those pure aerosol particles which make up the components of the various aerosol mixture models. During the retrieval process, the modified linear-mixing method is then used to simulate the reflectances of the candidate aerosol mixtures which potentially exist at the time and location of the observation. The retrieval process solves for the best-fitting optical depth of each aerosol mixture and determines those mixtures which give the smallest residuals in comparison to the observations, using a variety of metrics to evaluate the goodness of fit.

The pure aerosol particles used in this work are listed in "Table 1. For the purposes of this paper,

we assumed these aerosols are spherical in shape and follow a log-normal size-distribution (however, for the models used in the MISR retrievals, the mineral dust scattering properties will be calculated using a theory appropriate for non-spherical particles [Mishchenko et al., 1996].) Since hygroscopic particles swell with increasing relative humidity (RH), the size-distribution, and therefore, the scattering and absorption properties of such particles, are assumed to be functions of RH. In calculating the reflectance of aerosol mixtures, the properties of the hygroscopic particles change with RH while those for the non-hygroscopic particles remain the same.

The phase functions, p_i , and single scattering albedos, ω_i , were calculated in MISR's four spectral bands, centered at 443 nm, 555 nm, 670 nm, and 865 nm, using Mie theory. The calculations were made at 0% relative humidity for all the particles, and additionally at 70%, 90% and 99% relative humidities for the hygroscopic particle types. Figure 1 shows the phase functions of these particles at 443 nm and at 70% relative humidity. Assuming a 2-layer atmosphere with the Rayleigh layer on the top and the pure aerosol particles on the bottom, ρ_i was calculated for each of the particles.

More than 40 aerosol models were created by mixing two or three of the pure aerosol particles in the combinations shown in Table 2. The models cover a wide range of τ_a (0.0 to 0.85 at 443 nm and at 70% RH). The effective phase function, P_{mix} and single scattering albedo, ω_{mix} , were calculated, using Eqs. (4) and (5), and the true atmospheric path equivalent reflectance, ρ_t , was then computed for each of the mixtures.

The value of ρ , for each of these models was then calculated by the modified linear-mixing method, using Eqs. (7), (8), and (9), and for comparison, by the standard method, using Eq. (1).

The calculations of the atmospheric path radiances were made for nine values of the aerosol optical thickness, τ_a , in the range from 0.05 to 2.0. We used a viewing geometry applicable to MISR, representative of all latitudes and seasons, which corresponds to the viewing angles, θ , of 0° (nadir) and 26.10° , 45.6° , 60.0° , and 70.50° (fore and aft of nadir) and to a set of 10 sun angles, ϕ , ranging from 18.3° to 78.5° . The values of $\Delta\phi$ vary from 210° to 257° .

The error, expressed as:

$$\Delta = \frac{\rho_t - \rho}{\rho_t}, \quad (10)$$

was then estimated, for both the standard and modified methods, for all of the models. Another method of evaluating the error is with respect to the instrument absolute radiometric uncertainty. The parameter δ is defined as:

$$\delta = \frac{\rho_t - \rho}{\sigma_{abs}}, \quad (11)$$

where σ_{abs} is an estimate of the absolute radiometric uncertainty of the instrument's observations (for MISR, σ_{abs} is specified to be 3% of the equivalent reflectance when $p = 1.0$) and 6% of the equivalent reflectance when $p = 0.05$). A value of $\delta < 1.0$ means that the linear-mixing approximation is indistinguishable from the true value to within the instrument's measurement accuracy.

The Results

The results are obtained for more than 40 models at MISR's four spectral bands and nine cameras at ten sun angles, and four values of the relative humidity, i.e. a total of more than 14,400 cases, each at nine optical depth values ranging from 0.05 to 2.0. A representative sample of these results is shown here.

As explained in the introduction, the standard linear-mixing does not account for the multiple interactions between the aerosol components. As a result, the standard method overestimates the atmospheric path radiance for aerosols which consist of weakly- or non-absorbing components mixed with strongly absorbing ones. Such models are usually characterized by large values for F (> 0.1). Figure 2 illustrates a comparison between p , as calculated by both the standard and the modified linear-mixing methods, and its true value, ρ_f , for two aerosol models which were created by mixing increasing amounts of Soot with Sulfate. The comparisons presented in figure 2 are made for nadir viewing with $\theta_0 = 78.5^\circ$ at $\lambda = 443$ nm and 865 nm, and at RH = 70%. As shown in this figure, the standard method overestimates the value of p , with respect to its true value ρ_f , and mm-c so for larger optical depth where multiple interactions among the aerosol components are significant. With the modified linear-mixing approach, this discrepancy is greatly reduced. The values of A , evaluated for both methods, are shown in figure 3 for a subset of MISR's viewing geometry which includes the extreme values of θ (0.0° and 70.5°) and θ_0 (18.0° and 78.5°). As shown in figure 3, the errors produced by the modified linear-mixing method are within -5% for all the four viewing geometries and up to $\tau_a = 2.0$. The standard method, however, achieves this accuracy only up to $\tau_a = 1.5$ for the weakly absorbing mixture ($\omega_{mix} = 0.98$, $\epsilon = 0.12$ at 443 nm and 70% RH), and up to $\tau_a = 0.5$ for the more absorbing mixture ($\omega_{mix} = 0.91$, $\epsilon = 0.38$).

Figure 4 illustrates the error A for two models which are characterized by $\epsilon < 0.1$. The values of ω_{mix} for these two models are 0.95 and 0.72 (at 443 nm), respectively indicating, weakly-absorbing and strongly-absorbing aerosols. As shown in figure 4, the errors produced by the modified method are within 4% for both models, at all the presented wavelengths and viewing geometries, and up to $\tau_a = 2.0$. The standard linear-mixing method achieves such accuracy for the model which has $\epsilon = 0.05$, though it is strongly absorbing.

When evaluated with respect to the absolute, radiometric uncertainty of the MISR instrument, the errors produced by the modified linear-mixing approach are mostly within $1 \sigma_{abs}$, and rarely $1.5 \sigma_{abs}$, for all the aerosols and viewing geometries, considered in this study, and up to optical depth of 2.0. Similar results are obtained with the standard method but only for models which have $\epsilon < 0.08$. Figures 5 and 6 show these errors for the same sample of models used in figures 3 and 4.

Conclusions

Aerosol linear-mixing is a method by which the atmospheric path radiance due to an aerosol mixture is estimated from the contributions of the individual aerosol components present in the mixture. The standard linear-mixing approach does not account for the multiple interactions between different aerosol components present in the mixture. When the scattering characteristics of these components are sufficiently different such that the parameter ϵ is larger than -0.1, their interactions can cause the standard linear-mixing method to fail. We present a modified linear-mixing approach which approximates the effect of the multiple interactions among the aerosol components. The modified method produces the atmospheric path radiance with errors $\leq 5\%$ for more than 40 aerosol models, which are characterized by a wide range of ϵ , for a wide range of viewing and sun angles and up to optical depth of 2.0. These errors, however, are mostly within the anticipated absolute radiometric uncertainty of MISR's observations.

Acknowledgment

This research was conducted at the Jet Propulsion Laboratory, California Institute of Technology, under contract with the National Aeronautics and Space Administration.

Table 1: Properties of the pure aerosol particles used in this investigation

Aerosol	r_c (μm)	σ (pm)	$n_r - n_i$	ω
Sulfate/nitrate	0.08	1.88	1.46 - (0.0)	1.00
Mineral Dust	0.47	2.51	1.53-0.008	0.81
Sea Salt	0.39	2.11	1.41 -0.0	1.00
Urban Soot	0.012	2.0	1.75-0.455	0.252
Biomass Burning	0.4	1.8	1.43-0.0035	0.93
Urban1 (W&G)	0.03	2.3	1.468-0.0536	0.737
Urban2 (W&G)	0.487	2.52	1.464-0.0519	0.54

1- The properties listed in the above table are given at $\lambda = 443 \text{ nm}$ and $\text{RH} = 70\%$.

2- r_c and σ are, respectively, the Characteristic radius and width for log-normal size distributions where the number of particles of radius r is given as:

$$n(r) = \frac{N}{(2\pi)^{0.5}} \frac{C \times p}{r \log \sigma} \exp \left(-\frac{(\log r - \log r_c)^2}{2(\log \sigma)^2} \right)$$

where, N is the total number of particles per unit volume.

3- n_r and n_i are, respectively, the real and imaginary part of the refractive index.

4- Urban1 and Urban2 (W&G) are the two strongly absorbing aerosols used by Wang and Gordon (1994).

Table 2: Aerosol mixtures used in this investigation

Aerosol	Component 1	Component 2	Component 3	ω_{mix}	ϵ
Clean Continental	Sulfate	Mineral Dust	Urban Soot	0.76-0.99	0.02 -0.4
Industrial Continental	Sulfate	Mineral Dust	Urban Soot	0.74-0.98	0.12-0.85
Bio Burn Continental	Sulfate	Mineral Dust	Biomass Burning	0.87-0.98	0.03-0.08
Clean Maritime	Sulfate	Sea Salt		1.0	0.0
Industrial Maritime	Sulfate	Sea salt	Urban Soot	0.87- 0.9	0.4- 0.6
Bio Burn Maritime	Sulfate	Sea Salt	Biomass Burning	0.99-0.997	0.01-0.02
Dusty Maritime	Sulfate	Sea Salt	Mineral Dust	0.95-0.98	0.03-0.01
Urban-Mix	Urban 1 (W&G)	Urban2 (W&G)		0.65 -0.72	0.05-0.15

1-A total of 43 aerosol models, several from each of the categories listed above, were created by mixing different amounts of 2 or 3 of the corresponding components. The models were created such that ω_{mix} and ϵ cover as wide ranges of values as possible.

2- The range of values for ω_{mix} and ϵ , listed in the above table, are given at $\lambda = 44311111$ and RH = 70%. W&G refers to aerosol models used by Wang and Gordon (1994).

Figure Captions

Figure 1: Phase function of the pure aerosol particles listed in table 1. The Urban 1 and Urban2 models (referenced by W&G) are similar to the 2 Urban models used by Wang and Gordon (1994).

Figure 2: Comparison of p as calculated by the standard and modified linear-mixing methods (the triangles and crosses, respectively) to the true value p_t (circles) for two aerosol models characterized by $\epsilon \geq 0.1$. p is presented for each of the two models as a function of the aerosol optical depth, τ_a , at 443 nm and 865 nm, for nadir viewing with sun angle $\theta_0 = 78.5^\circ$ and RH = 70%. Note that in figure 2, and the subsequent figures, the mixing ratios are expressed as the fractional contributions of the aerosol components to the total optical depth τ_a and that, for the same model, they vary with wavelength.

Figure 3: The error, A (%) of the standard (triangles) and modified (crosses) linear-mixing methods for aerosol models characterized by $\epsilon \geq 0.1$. The results are shown as functions of the aerosol optical depth, τ_a , for the four viewing geometries, described by the view angles $\theta = 0.0$ and 70.5° , each at the sun angles $\theta_0 = 18.0^\circ$ and 78.5° , and at RH = 70%. Note change in scale for different panels.

Figure 4: The errors, A (%) of the standard (triangles) and modified (crosses) linear-mixing methods for aerosol models characterized by $\epsilon < 0.1$. The results are shown as functions of the aerosol optical depth, τ_a , for the four viewing geometries, described by the view angles $\theta = 0.0$ and 70.5° , each at the sun angles $\theta_0 = 18.0^\circ$ and 78.5° , and at RH = 70%. Note change in scale for different panels.

Figure 5: The error, δ , of MISR's observations, for aerosol models characterized by $\epsilon \geq 0.1$. The results are shown as functions of the aerosol optical depth, τ_a , for the four viewing geometries, described by the view angles $\theta = 0.0$ and 70.5° , each at the sun angles $\theta_0 = 18.0^\circ$ and 78.5° , and at RH = 70%. Note change in scale for different panels.

Figure 6: The error, δ , of MISR's observations, for aerosol models characterized by $\epsilon < 0.1$. The results are shown as functions of the aerosol optical depth, τ_a , for the four viewing geometries, described by the view angles $\theta = 0.0$ and 70.5° , each at the sun angles $\theta_0 = 18.0^\circ$ and 78.5° , and at RH = 70%. Note change in scale for different panels.

References

Diner, D. J., W. A. Abdou, C. J. Bruegge, J. E. Conel, R. A. Kahn, J. V. Martonchik, S. R. Paradise, and R. A. West, Status of the Multi-angle imaging SpectroRadiometer instrument for EOS-AM 1 and its application to remote sensing of aerosols, Proceedings of the IGARSS Symposium, Florence, Italy (1995).

Diner, D. J., C. J. Bruegge, J. V. Martonchik, G. W. Bothwell, E. D. Danielson, V. G. Ford, I. E. Hovland, K. L. Jones, M. L. White, A Multi-angle Imaging SpectroRadiometer for terrestrial remote sensing from the Earth observing System, Internatl. J. imaging Sys. and Tech. 3, **92-107** (1991).

Jansen, J. E. and I. D. Travis, Light scattering in planetary atmospheres, Space Sci. Rev. 16, 527-610 (1974).

Mishchenko, M. I., I. D. Travis, R. A. Kahn, and R. A. West, Modeling phase functions for dust-like tropospheric aerosols using a shape mixture of randomly oriented polydisperse spheroids, submitted to J. Geophys. Res. (1996).

Wang, M. and H. R. Gordon, "Radiance reflected from the ocean-atmosphere system: synthesis from individual components of the aerosol size distribution, Appl. opt. 33, 7088-7095 (1994).

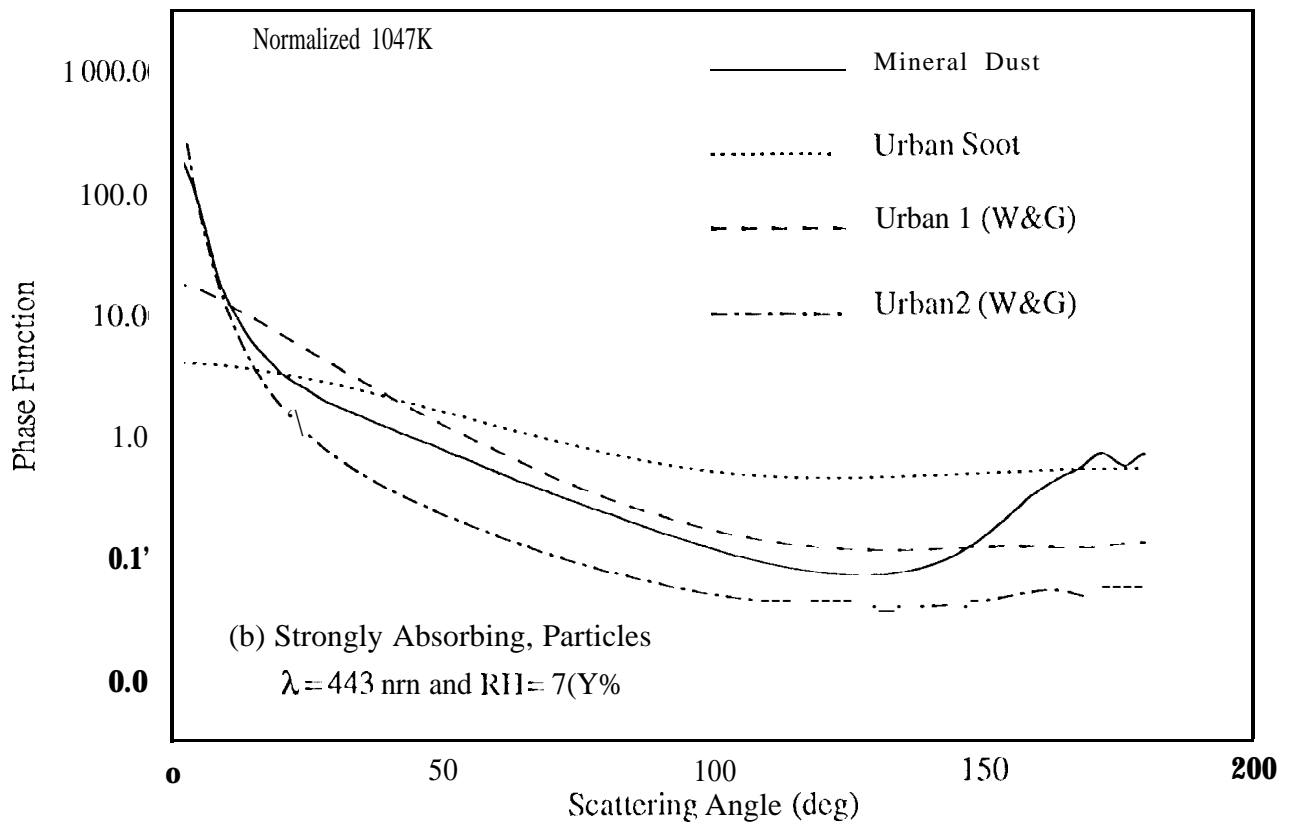
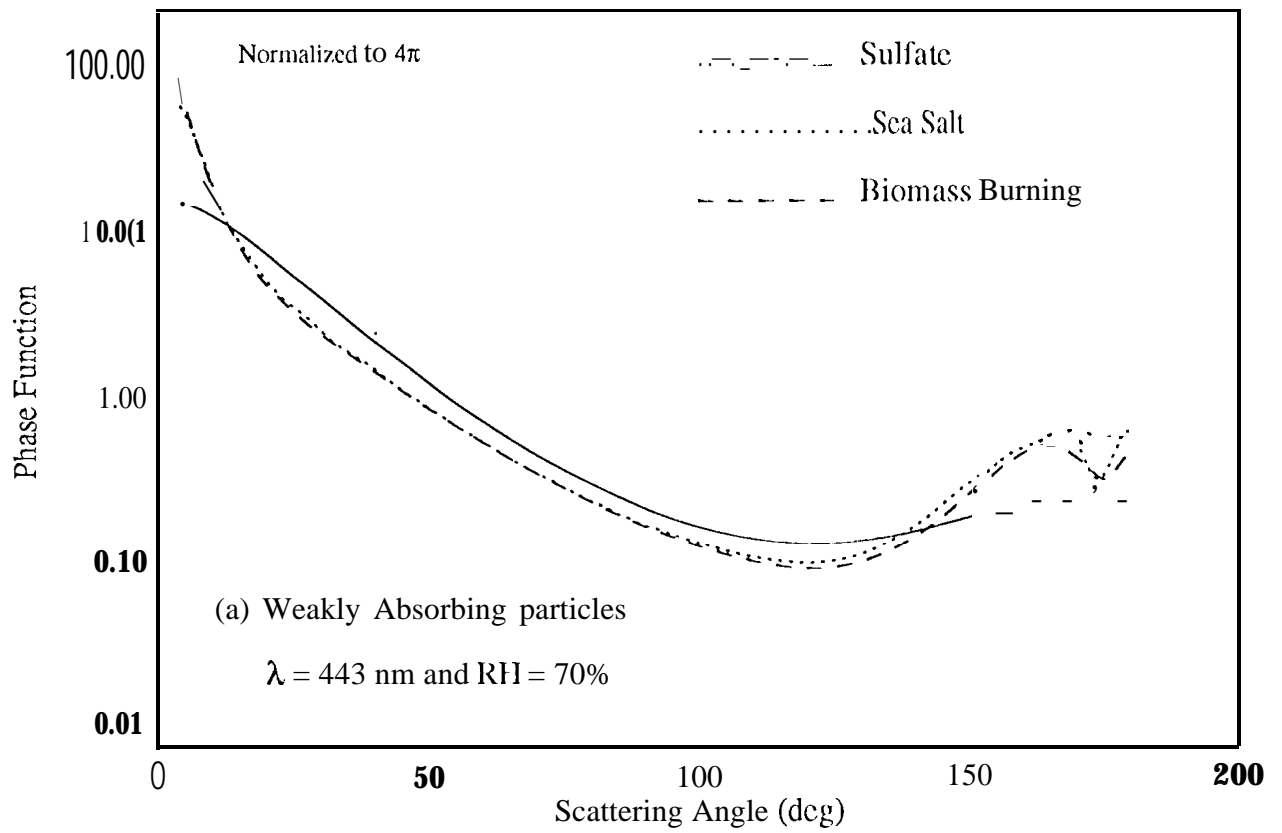


Figure 1.

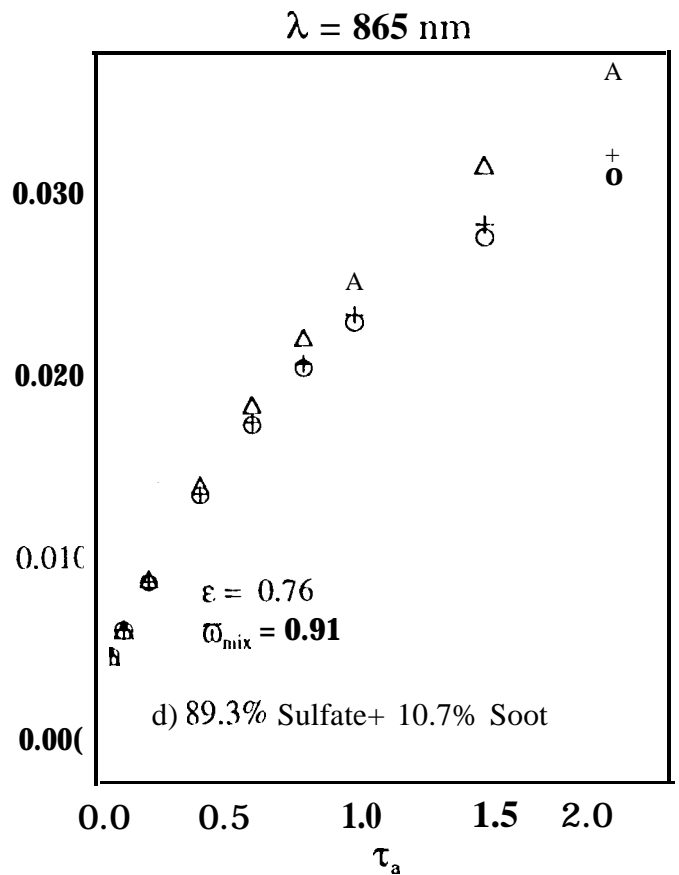
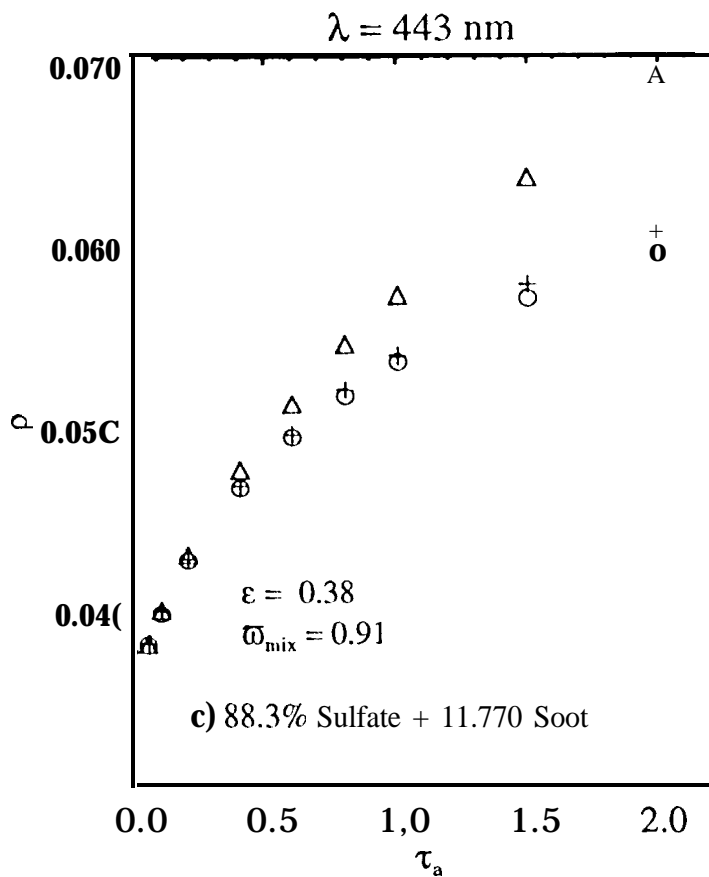
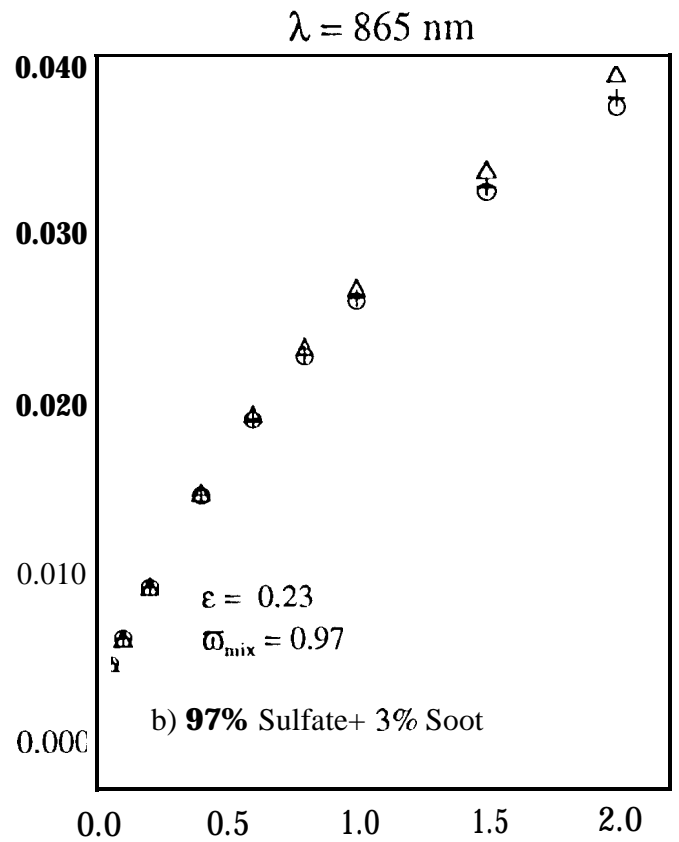
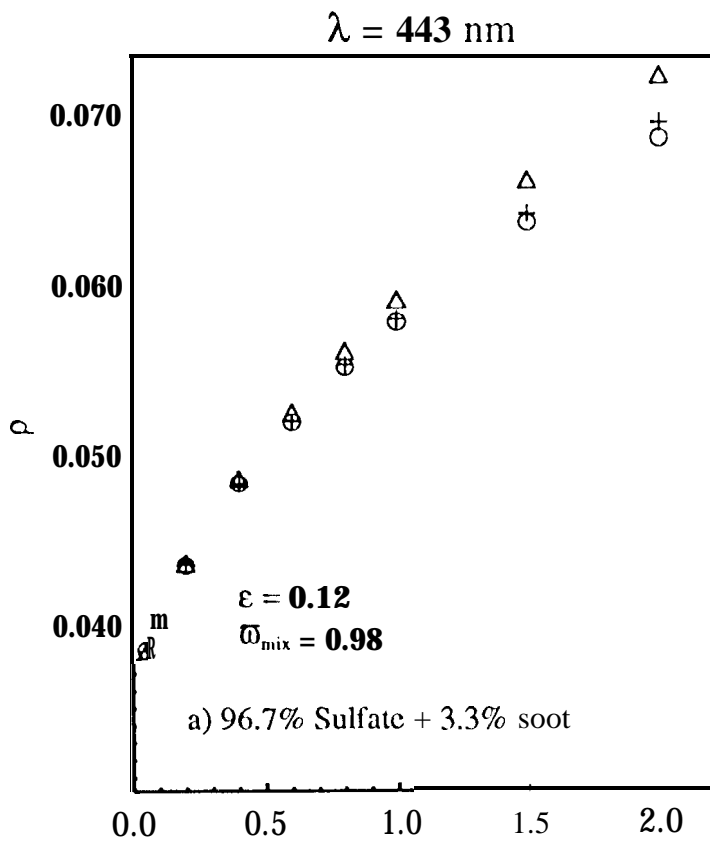


Figure 2.

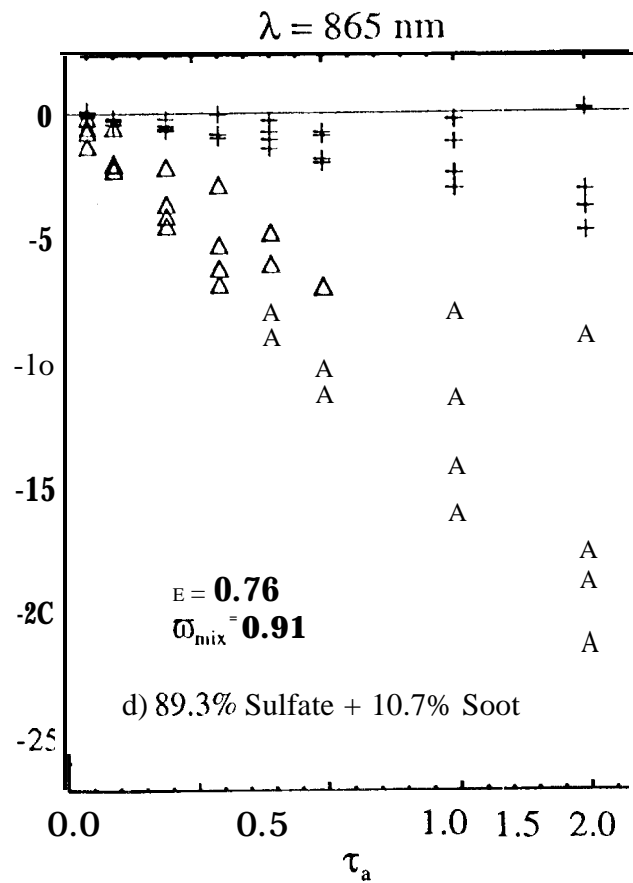
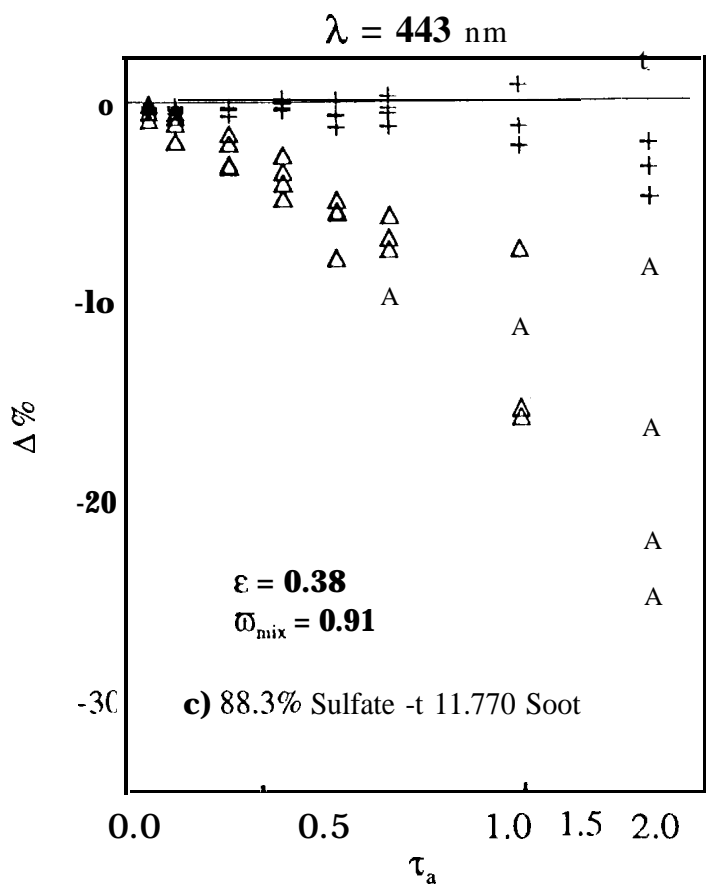
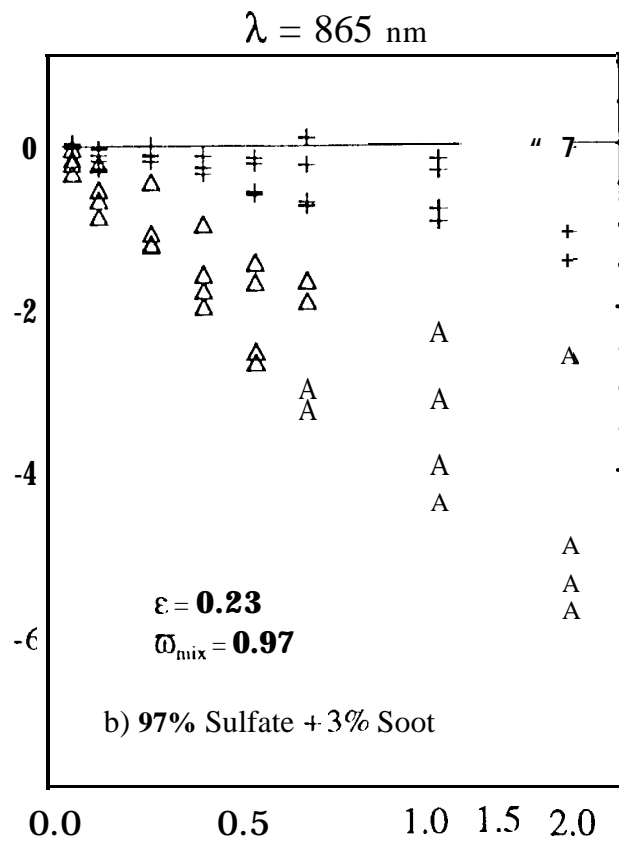
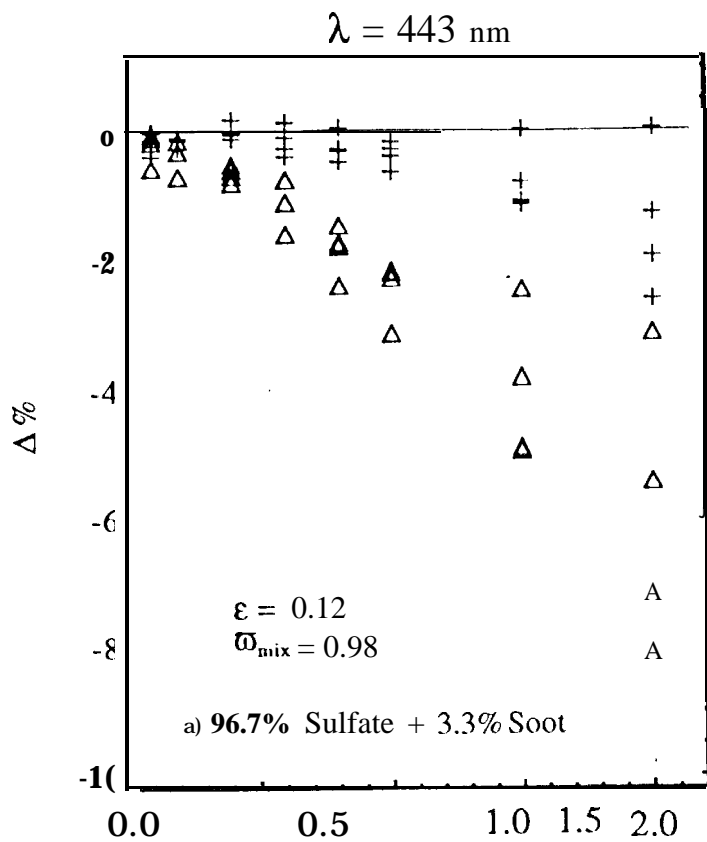


Figure 3.

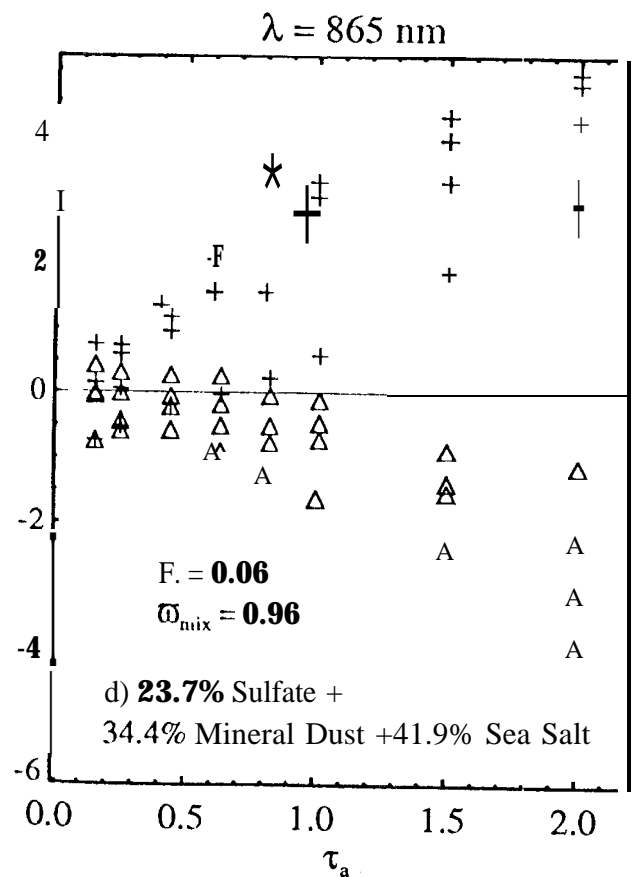
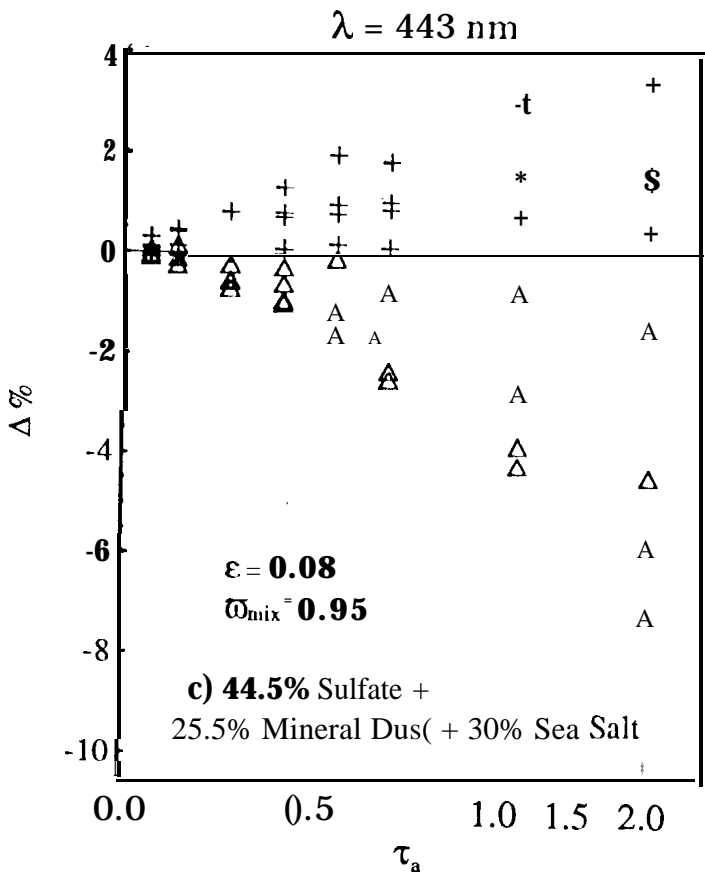
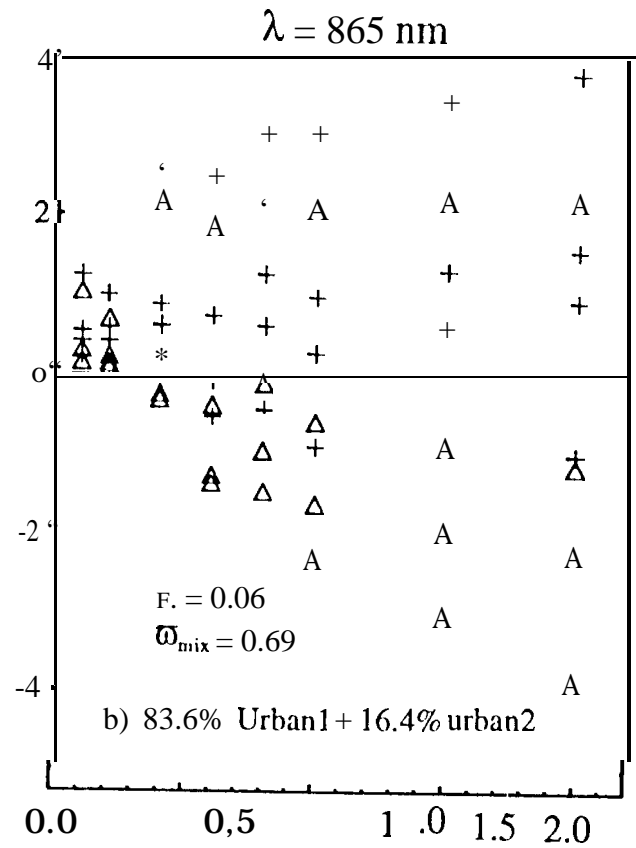
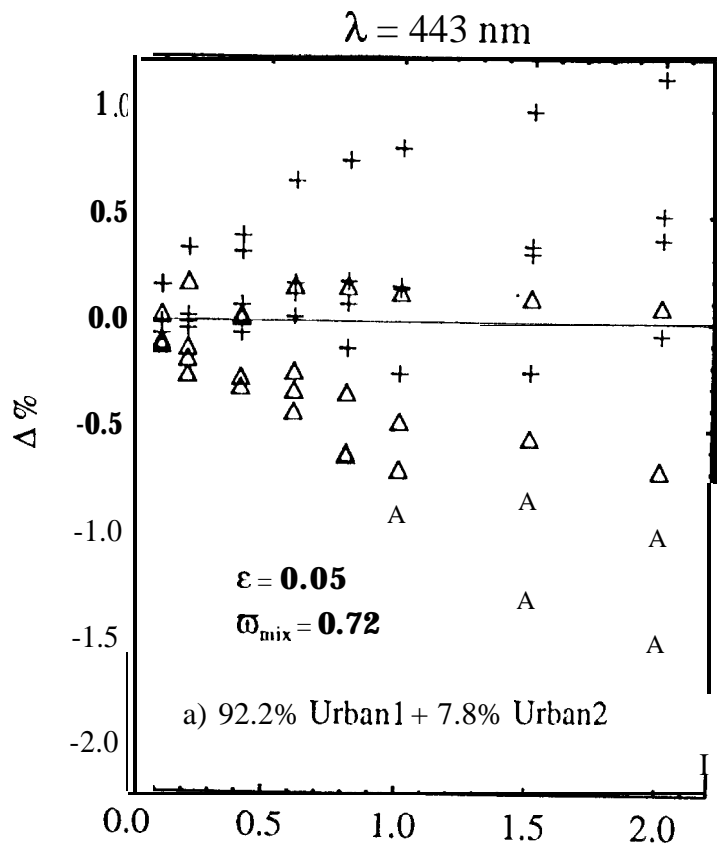


Figure 4.

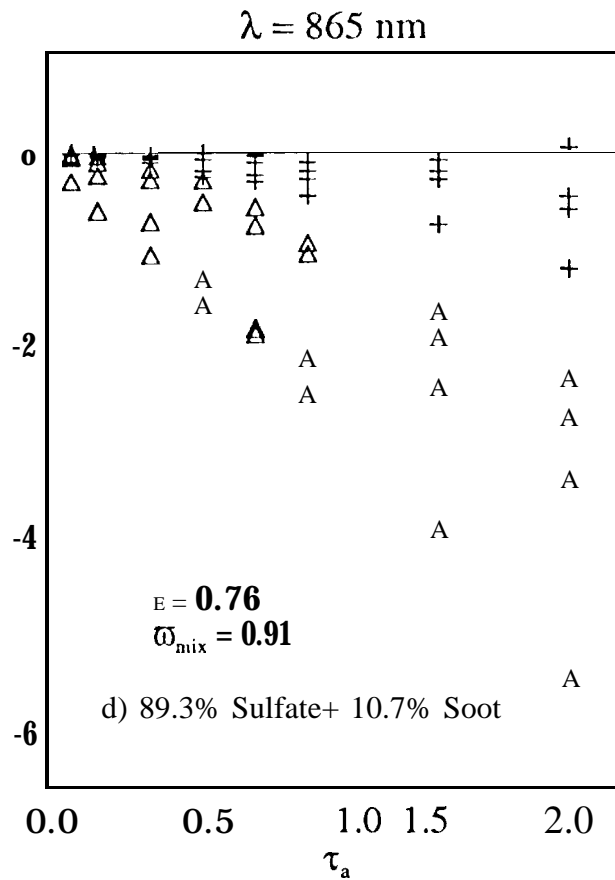
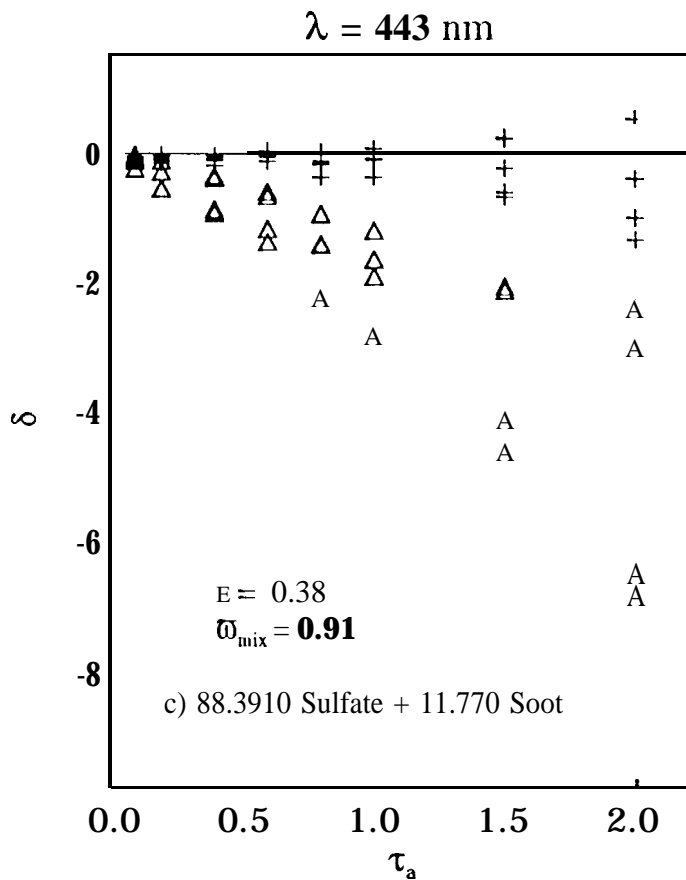
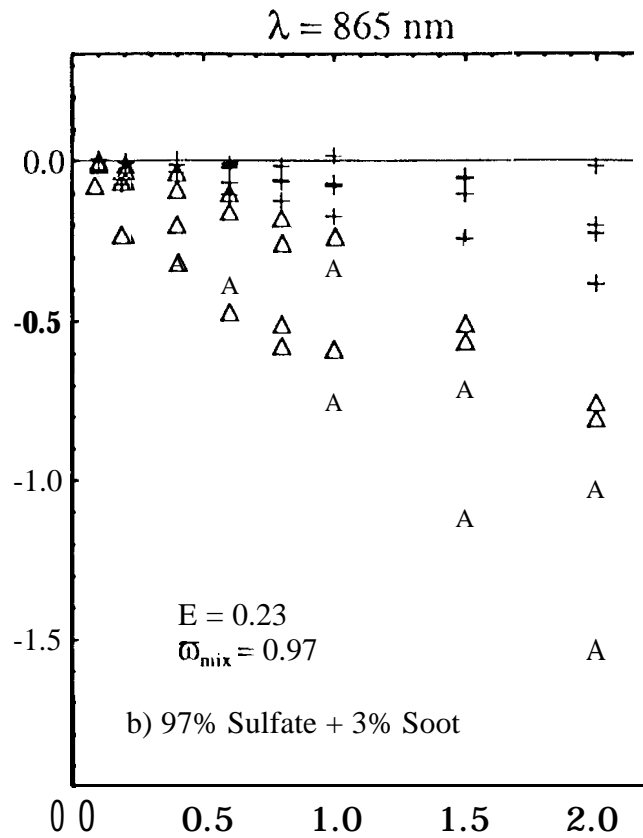
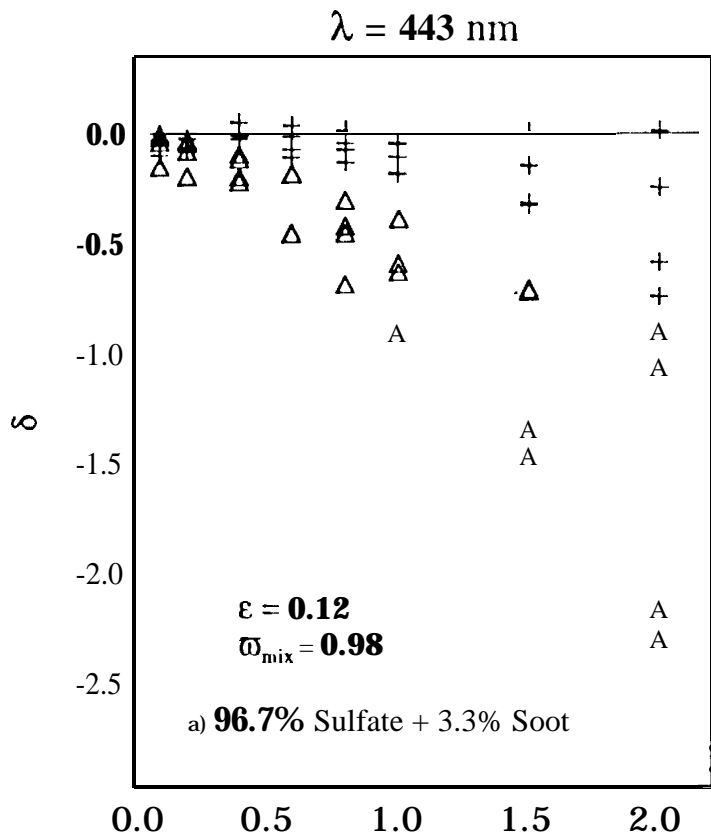


Figure. 5.

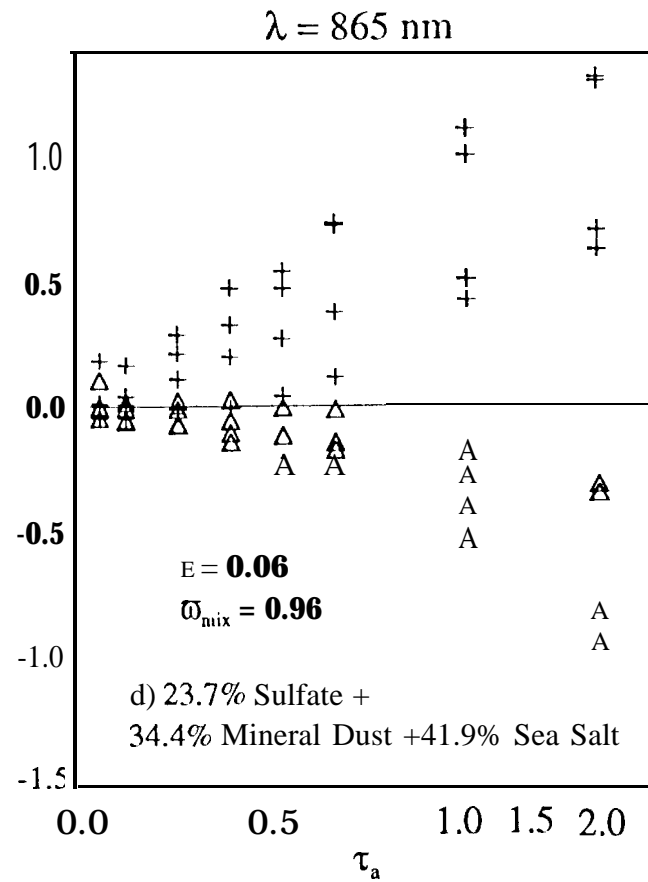
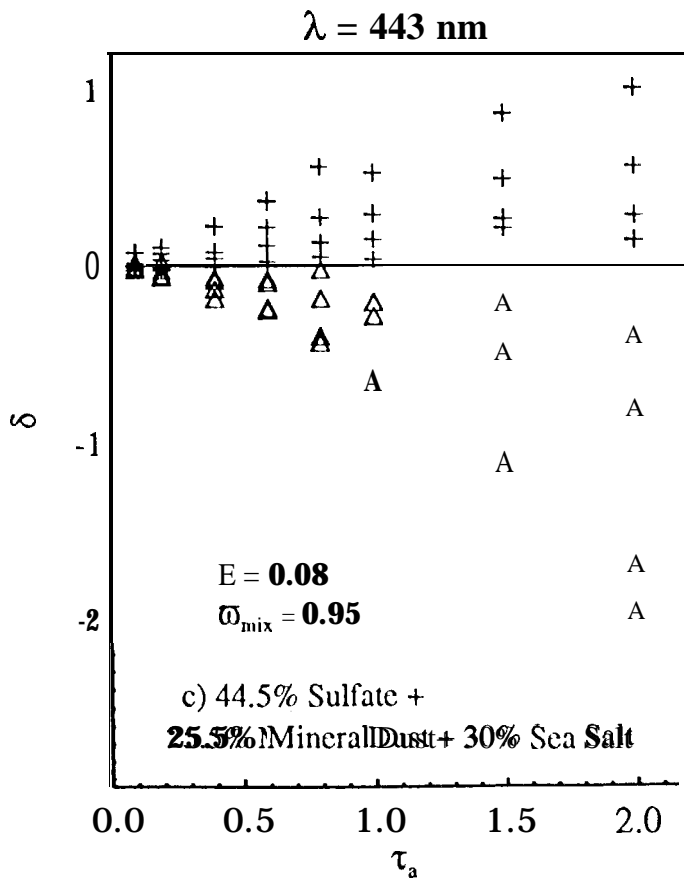
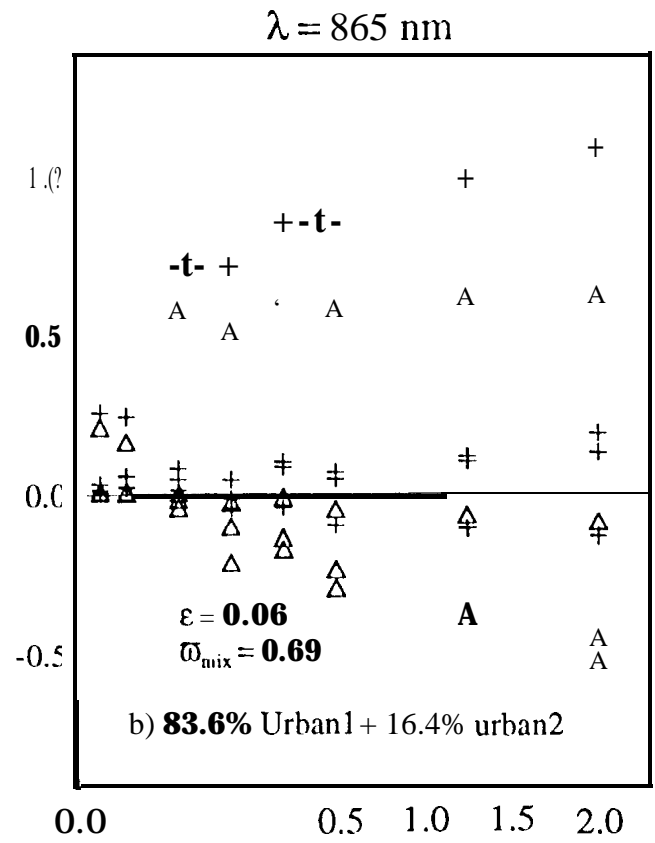
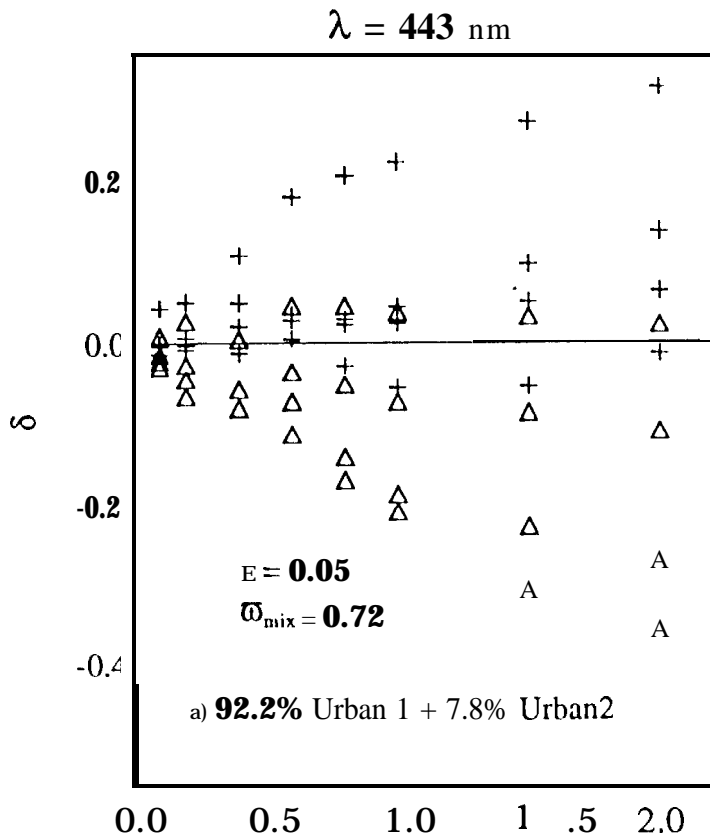


Figure 6.